# Identification of a biosynthetic gene cluster encoding a novel lanthanide chelator in *Methylorubrum extorquens* AM1

Alexa M. Zytnick[a], Nathan M. Good[a], Colin C. Barber[a], Manh Tri Phi[b], Sophie M. Gutenthaler[b], Wenjun Zhang[c], Lena J. Daumann[b], and N. Cecilia Martinez-Gomez[a,1]

[a]Department of Plant and Microbial Biology, University of California, Berkeley, Berkeley, California, USA

[b]Department of Chemistry, Ludwig-Maximilians-Universität München, München, Germany.

[c]Department of Chemical and Biomolecular Engineering, University of California, Berkeley, Berkeley, California, USA

[1]**Email:** cecimartinez@berkeley.edu

**Author contributions:** Conceptualization, A.M.Z., N.M.G., and N.C.M.G.; methodology, A.M.Z, C.C.B, M.T.P., and S.M.G; investigation, A.M.Z. and C.C.B; writing - original draft, A.M.Z., N.M.G., and N.C.M.G.; writing - reviewing and editing, N.M.G., N.C.M.G., W.Z., and L.J.D.; funding acquisition, N.C.M.G. and L.J.D.; resources, N.C.M.G., W.Z., and L.J.D.

N.C.M.G., N.M.G. and A.M.Z. are inventors on patent application B22-074 submitted by the Regents of the University of California**.**

**Competing interest statement:** The authors declare no competing financial interest(s).

**Keywords:** Lanthanides, Metals, Methylotrophy, Rare Earth Elements

## ABSTRACT

While lanthanide-dependent metabolism is widespread in nature and has been proven to drive one-carbon metabolism in bacteria, details about the machinery necessary to sense, sequester, and traffic lanthanides (Ln) remain unknown. This gap in knowledge is in part because nearly all bacterial growth studies with Ln to date have used soluble chloride salts, compounds that do not reflect the insoluble Ln sources common in the natural environment. Here, we describe the changes in the metabolic machinery of *Methylorubrum extorquens* AM1 in response to poorly soluble $Nd_2O_3$, including 4-fold increases in orphan *pqqA* genes and the Ln-dependent ADHs *xoxF1* and *exaF* compared to growth with soluble $NdCl_3$. We report the first description of a Ln-chelator biosynthetic gene cluster, encoded by META1p4129 through META1p4138 that we named the Lanthanide Chelation Cluster (LCC). The LCC encodes a TonB dependent receptor and NRPS biosynthetic enzymes and is predicted to produce a metal-chelating molecule. As some LCC protein sequences share similarity to biosynthetic enzymes producing the Fe-chelating siderophore aerobactin, the capacity of aerobactin for binding Ln was tested. It was found that while aerobactin can bind lanthanum (La), neodymium (Nd) and lutetium (Lu) at physiological pH, providing only exogenous aerobactin did not affect growth rate or yield. The LCC was highly upregulated when *M. extorquens* AM1 was grown using $Nd_2O_3$ and expression *in trans* enabled an increase of Nd bioaccumulation by over 50%. Expression of the LCC *in trans* did not affect iron bioaccumulation, providing further evidence that its product is a novel Ln-chelator. Finally, expression of the LCC *in trans* increased Nd, dysprosium (Dy), and praseodymium (Pr) bioaccumulation from the complex Ln source NdFeB magnet swarf by over 60%, opening new strategies for sustainable recovery of these critical Rare Earth Elements.

## INTRODUCTION

Metal ions are essential for life–serving in catalytic and structural roles, metal ions are intrinsically involved in many biological processes including respiration, DNA replication, and biosynthesis of metabolic intermediates. The importance of metal ions for life processes is further underscored by the evolution of elegant systems for acquisition and transport. It is estimated that ~40-50% of all enzymes in existence require a metal ion for proper function (1–3), yet metals can be biologically inaccessible in most natural environments. One such metal is iron, which predominantly exists as insoluble ferric ($Fe^{3+}$) oxides in the environment (4). To increase bioavailability of this essential cofactor, microorganisms have evolved to secrete Fe-chelating small molecules known as siderophores (Greek: iron carrier). Biosynthesized primarily through nonribosomal peptide synthetase (NRPS) and polyketide synthase (PKS) systems, siderophores fall into five classes based on their Fe-binding moieties: catecholate, phenolate, hydroxamate, carboxylate, and diazeniumdiolate (5, 6). In Gram-negative bacteria, TonB complexes provide the energy for siderophore-bound Fe to be brought into the periplasm via an outer-membrane beta-barrel receptor. An ABC transporter then facilitates the transfer of the complex to the cytoplasm, where the siderophore can be recycled for subsequent iterations of this process or can undergo hydrolysis to release its cargo (7–9).

Like Fe, Ln (light, atomic numbers 57-62; and heavy, atomic numbers 63-71) are established members of the metal ions used for life processes. As “new life metals,” little is known of how bacteria acquire these poorly bioavailable elements (10–12). The interaction of siderophores with Ln has been studied extensively *in vitro*. Tircsó *et al.* explored the coordination chemistry of gadolinium ($Gd^{3+}$), $Nd^{3+}$, and ytterbium ($Yb^{3+}$) with desferrioxamine B and desferricoprogen as possible contrast agents for MRI (13). To elucidate biological f-element trafficking mediated by

siderophores and siderophore binding proteins, Abergel *et al.* investigated the interactions of enterobactin and siderocalin with samarium ($Sm^{3+}$), europium ($Eu^{3+}$), $Gd^{3+}$, and actinides (14). Additionally, Raymond *et al.* have shown that hydroxamate and catecholate siderophore inspired ligands can be used to coordinate a variety of Ln (15). While these studies have elucidated siderophore-Ln interactions *in vitro*, it is not known if siderophores or as of yet unknown metallophores are responsible for solubilizing Ln *in vivo*.

In a biological context, Ln are best understood for their function in the cofactor complex of some periplasmic alcohol dehydrogenases (ADHs). These enzymes generate catalytic activity via a Ln:pyrroloquinoline quinone (PQQ) cofactor complex coordinated in the active site (16, 17). PQQ is not restricted to prokaryotic enzymes and can be found in all three domains of life (18, 19). Ln:PQQ-enzymes are likely more important to natural processes than we currently understand them to be. Ln:PQQ-dependent ADHs are exemplified by XoxF methanol dehydrogenases (MDHs), of which there are five distinct phylogenetic clades distributed among methylotrophic bacteria (20), and ExaF ethanol dehydrogenase (EtDH), discovered in the methylotrophic bacterium *Methylorubrum extorquens* AM1 (21). The discovery of Ln:PQQ-dependent enzymes has led to the reclassification of some organisms as true methylotrophs, such as *Bradyrhizobium japonicum* (22), the discovery of new methylotrophs (23), and the discovery of Ln:PQQ-dependent enzymes in non-methylotrophs, such as PedH EtDH (24).

Ln must enter the periplasm in *M. extorquens* to be used by Ln:PQQ-dependent enzymes, but the details for acquisition and transport of Ln are not entirely understood. A gene cluster encoding a TonB-dependent receptor and an ABC-transport system important for Ln utilization and transport (*lut*) was discovered and characterized in *M. extorquens* AM1 (25) and the closely related phyllosphere isolate *M. extorquens* PA1 (26). Even though XoxF and ExaF ADHs are

periplasmic enzymes with Sec pathway signal peptides, Ln must be transported to the cytoplasm, via the *lut*-encoded ABC transport system for the cell to be able to grow if methanol oxidation is reliant on a Ln-dependent enzyme (25, 26). The necessity of Ln reaching the cytoplasm is not completely understood. However, the presence of exogenous Ln generates a transcriptional response resulting in the switch from the calcium (Ca):PQQ MDH, MxaFI, to the Ln-dependent XoxF MDH.

During methylotrophic growth, *M. extorquens* AM1 has been demonstrated to use complex, insoluble Ln sources such as computer hard drive magnets to supply these enzymes with their Ln cofactor (27). In natural, non-extreme environments, Ln are most often found in highly insoluble oxide and phosphate forms, usually in minerals and ores such as monazite and bastnäsite (28), though extreme environments, such as volcanic mud pot water, with high temperatures and low pH, can contain relatively higher levels (micromolar range) of soluble Ln (10). The ability for methylotrophs to thrive in environments rich in complex and poorly soluble Ln sources suggests that a secreted, highly selective Ln-chelator, a "lanthanophore," could provide a biological mechanism for acquiring these metals in nature, but the details of Ln solubilization remain unknown. Though PQQ is secreted (29), has been shown to directly bind Ln (30), and its production is increased when Ln accumulation is elevated during certain growth conditions in *M. extorquens* AM1 (31), direct binding of PQQ with Ln for uptake has not been shown.

In this study, we assessed the impact of Ln solubility on the transcriptional response and ability of *M. extorquens* AM1 to grow on methanol and acquire Nd (atomic number 60) using sources of high ($NdCl_3$) and low ($Nd_2O_3$) solubility. We found growth with $Nd_2O_3$ was slower than with $NdCl_3$ and used RNAseq transcriptomics to identify the genetic basis for this difference. We identified increased expression of alternative methanol oxidation systems, PQQ biosynthesis, and

*lut* genes, consistent with metabolic alterations in response to the reduced solubility of $Nd_2O_3$. We also identified a gene cluster conserved across methylotrophs predicted to encode a metal chelating molecule that was upregulated during growth with $Nd_2O_3$. Expression of these genes *in trans* increased growth and Ln bioaccumulation from pure Nd sources and from complex NdFeB magnet swarf.

## RESULTS

***Ln solubility differentially regulates the Ln metabolic network.*** The presence of light Ln in methanol growth medium effects the regulatory switch from Ca-dependent MxaFI MDH to Ln-dependent XoxF MDH (32), but otherwise generates only modest alterations to growth rate, growth yield, and down-regulation of PQQ biosynthesis genes (32, 33). However, in these studies only soluble chloride compounds of light Ln were tested. To better understand the impacts of Ln solubility on methylotrophy in *M. extorquens* AM1, we measured methanol growth with soluble $NdCl_3$, and poorly soluble $Nd_2O_3$ using Δ*mxaF*, a strain that lacks catalytically active MxaFI. Comparing growth on $NdCl_3$ to $Nd_2O_3$, Ln solubility affected methanol growth of *M. extorquens* AM1, resulting in significantly faster growth ($p$ value < 0.0005) and better yield ($p$ value < 0.05) (Fig. 1*A*). To gain further insight into how methanol oxidation and Ln utilization machinery respond to Ln solubility, RNA-seq transcriptomics was employed to uncover mechanistic differences between these conditions. Using stringent cut-offs of |log2(fold change)| > 1 and $p$ < 0.0000005, we identified 1,468 differentially expressed genes (DEGs) between the $NdCl_3$ and $Nd_2O_3$ conditions (Fig. 1*B*, Fig. S1).

Upregulation of Ln-dependent MDH *xox* genes generated by the presence of exogenous $LaCl_3$ has been studied (33–36). Here, when $Nd_2O_3$ was provided the genes *xoxF1*, *xoxG*, and *xoxJ*

(respectively encoding the primary Ln-dependent MDH, its cognate cytochrome, and a MxaJ-like accessory protein) were among the most upregulated DEGs, exhibiting 5-fold increases when compared to the soluble Ln condition (Fig. 1*C*). Encoding the Ln-dependent EtDH, *exaF*, was shown to have a 3-fold increase in expression during growth with $Nd_2O_3$ compared to growth with $NdCl_3$, suggesting that alternative Ln-ADHs are important when Ln are less bioavailable. The use of alternative Ln-ADHs during growth with heavier Ln, e.g., Gd, has been shown previously (31). Additionally, *mxaG*, *mxaJ*, and *mxaI*, encoding the Ca-dependent MDH MxaFI's cognate cytochrome, a periplasmic solute binding protein, and the small MDH subunit, were downregulated ~2-fold on average during growth with $NdCl_3$ compared to growth of wild type in the absence of Ln (Table S1).

Previous studies have shown that although upregulation of *xoxF1* occurs as a response to soluble Ln, concomitant upregulation of the PQQ biosynthetic genes does not occur (33, 35). Similarly, most of the genes encoding the PQQ biosynthetic machinery were not significantly upregulated in the $NdCl_3$ condition in this study. Interestingly, *pqqA2* and *pqqA3* were upregulated 4-fold in the $NdCl_3$ condition compared to the $Nd_2O_3$ condition (Fig. 1*C*), indicating possible changes to PQQ production. Internal concentrations of PQQ were measured in cell extracts from cultures grown in both conditions to determine the correlation between the transcript profile and production of PQQ. Cell lysates from cultures grown with $NdCl_3$ contained significantly more PQQ (120 mM ± 29 mM) than lysates of cultures grown with $Nd_2O_3$ (24 mM ± 28 mM). This result suggests that PqqA levels and activity are likely limiting factors for PQQ biosynthesis.

The *lut* cluster, which encodes a TonB dependent transporter, an ABC transport system, and various periplasmic proteins, is essential for light Ln transport. Previous work has shown expression of *lutH* does not change in response to soluble $LaCl_3$ (33). In this study, *lutH* was

downregulated 9-fold in the $NdCl_3$ condition compared to the no Ln condition (Table S3) and upregulated 9-fold to the $Nd_2O_3$ condition denoting tight regulation of the TonB dependent transporter based on solubility and Ln species (Fig. 1*C*). The remaining *lut* genes exhibited 2-fold upregulation on average during growth with $Nd_2O_3$.

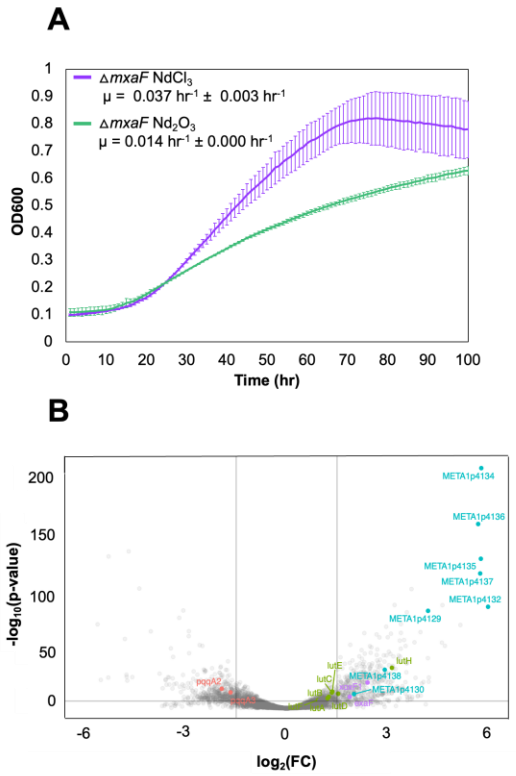


C

| function | locus tag | $log_2$ fold change | q value |
|---|---|---|---|
| Xox-type MDH | *xoxF1* (META1p1740) | 2.4 | 4.2E-22 |
| | *xoxF2* (META1p2757) | 0.2 | 4.5E-01 |
| | *xoxG* (META1p1741) | 2.8 | 4.6E-18 |
| | *xoxJ* (META1p1742) | 2.6 | 9.5E-23 |
| Mxa-type MDH | *mxaF* (META1p4538) | 0.0 | 1.0E00 |
| | *mxaG* (META1p4536) | 0.3 | 1.1E-01 |
| | *mxaJ* (META1p4537) | 0.5 | 3.7E-03 |
| | *mxaI* (META1p4535) | 0.2 | 3.6E-01 |
| Exa-type ADH | *exaF* (META1p1139) | 1.9 | 6.2E-10 |
| | *exaJ* (META1p1137) | 0.7 | 3.9E-02 |
| | *exaG* (META1p1138) | 0.3 | 2.2E-01 |
| PQQ biosynthesis | *pqqE* (META1p1748) | -0.3 | 6.7E-02 |
| | *pqqCD* (META1p1749) | 0.0 | 9.3E-01 |
| | *pqqB* (META1p1750) | -0.5 | 1.5E-02 |
| | *pqqF* (META1p2330) | -0.5 | 2.3E-03 |
| | *pqqG* (META1p2331) | -0.4 | 2.7E-02 |
| | *pqqA1* (META1p1751) | -0.8 | 5.1E-04 |
| | *pqqA2* (META1p4628) | -1.9 | 1.1E-16 |
| | *pqqA3* (META1p4629) | -1.6 | 1.3E-13 |
| *lut* cluster | *lutA* (META1p1778) | 1.2 | 1.2E-08 |
| | *lutB* (META1p1779) | 1.3 | 5.8E-10 |
| | *lutC* (META1p1780) | 1.3 | 1.8E-13 |
| | *lutD* (META1p1781) | 1.5 | 1.6E-12 |
| | *lute* (META1p1782) | 1.4 | 2.4E-14 |
| | *lutF* (META1p1783) | 0.9 | 3.2E-07 |
| | *lutG* (META1p1784) | 1.0 | 7.4E-07 |
| | *luth* (META1p1785) | 3.1 | 1.3E-34 |
| | *lanM* (META1p1786) | 0.9 | 5.6E-04 |
| | *lutI* (META1p1787) | -0.1 | 7.0E-01 |

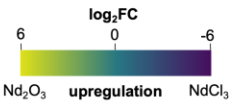


**Figure 1. Differences in Ln source solubility affect growth and transcriptional response of *M. extorquens*.** *A*) Growth rate of Δ*mxaF* is significantly increased during growth on soluble $NdCl_3$ (purple) compared to poorly soluble $Nd_2O_3$ (green). Individual data points represent the mean of three replicates. *B*) Volcano plot of DEGs comparing $NdCl_3$ and $Nd_2O_3$ conditions. Vertical lines signify cutoffs of < -1 and > 1 for $log_2$-transformed fold changes ($log_2FC$), while the horizontal line signifies a cutoff of *p* value < 0.0000005. *lut* cluster (green), PQQ

biosynthesis (red), Ln-dependent ADH (purple), and uncharacterized biosynthetic cluster genes (blue) are highlighted. *C*) Table depicting transcriptomic differences between ADH, PQQ biosynthesis, and *lut* cluster genes between $NdCl_3$ and $Nd_2O_3$ conditions. *q* values represent false discovery rate-adjusted *p* values.

***Ln solubility differentially regulates a putative siderophore biosynthetic gene cluster.*** Of the DEGs identified in RNAseq analysis, the genes META1p4129 through META1p4138 were the most highly upregulated in the $Nd_2O_3$ condition, with an average increase in expression of 32-fold compared to growth with $NdCl_3$ (Fig. 2*A*). Based on local alignment and HMM modeling, the cluster is composed of a TonB dependent receptor, regulatory elements, biosynthetic machinery, and hypothetical proteins (Fig. 2*A)*. The genome mining tool antiSMASH predicts the product of the biosynthetic gene cluster (BGC) to be a siderophore, yet the cluster lacks high homology to other siderophore BGCs in the antiSMASH repository. Phyre2 homology modeling of these gene products corroborates antiSMASH analysis, identifying genes in the cluster as siderophore biosynthesis components (Fig. 2*A)*. This cluster encodes an NRPS system, which is the most common biosynthetic route for siderophores. Furthermore, META1p4132 has 98% sequence identity to the aerobactin synthesis gene *iucA* and Phyre2 homology modeling exhibits 100% confidence in this classification (Fig 2*A*).

Presence and similarity of the cluster across the RefSeq non-redundant protein record was determined using the cblaster and clinker pipelines (37, 38). The gene cluster is highly conserved across *Methylorubrum* and *Methylobacterium* species. Some elements of the cluster are conserved in distantly related proteobacteria, such as *Rhodopseudomonas palustris* and *Hyphomicrobiales bacterium*. Interestingly, the cluster is also present in *Phreatobacter stygius,* a non-methylotroph member of *Rhizobiales* which lacks the remaining necessary genes for

aerobactin synthesis (Fig. 2*B*). The insights that the gene cluster is a) conserved across methylotrophs, b) predicted to encode a metal chelator, and c) upregulated during growth with an insoluble Ln source, all suggest that the cluster may play a critical role in Ln solubilization. For these reasons we have named this gene cluster the LCC for "Lanthanide Chelation Cluster"

**A**

| locus tag | $log_2$ fold change | q value | BLASTP next related protein | identity | coverage | Phyre2 model | confidence | coverage |
|---|---|---|---|---|---|---|---|---|
| META1p4129 | 4.2 | 3.7E-84 | TonB dependent receptor | 98.8% | 100% | TonB-dependent receptor | 100% | 89% |
| META1p4130 | 2.0 | 3.0E-12 | Transmembrane sensor | 99.7% | 100% | Siderophore interacting protein | 100% | 64% |
| META1p4131 | 6.1 | 3.6E-58 | RNA polymerase sigma factor | 100% | 100% | RNA polymerase sigma factor | 99.9% | 97% |
| META1p4132 | 6.0 | 1.2E-87 | Siderophore synthetase component | 99.8% | 98% | Aerobactin synthase lucA | 100% | 92% |
| META1p4133 | 6.3 | 1.1E-165 | Putative NRPS | 100% | 99% | Desferrioxamine biosynthesis protein | 100% | 55% |
| META1p4134 | 5.8 | 3.62E-209 | DUF6005 family protein | 97.7% | 100% | Oxidoreductase | 98.8% | 19% |
| META1p4135 | 5.8 | 8.3E-130 | Xylose isomerase | 100% | 20% | Lyase | 99.1% | 20% |
| META1p4136 | 5.7 | 3.2E-160 | DUF2218 family protein | 97.8% | 100% | Hypothetical protein | 100% | 100% |
| META1p4137 | 5.8 | 6.8E-117 | GNAT family acetyltransferase | 99.4% | 94% | Acetyltransferase | 100% | 94% |
| META1p4138 | 2.9 | 6.1E-33 | Putative outer membrane protein | 99.6% | 100% | Putative secreted protein | 100% | 68% |

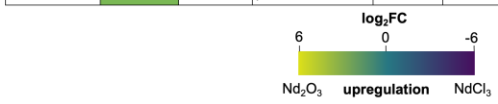


**B**

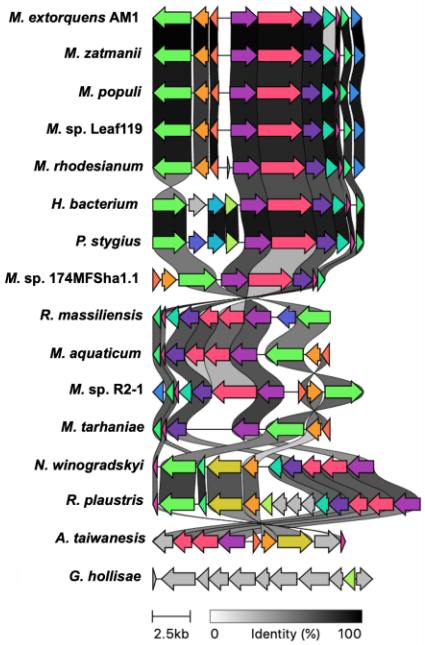


**Figure 2. LCC bioinformatic characterization.** *A*) Table depicting upregulation of META1p4129 through META1p4138 during growth with $Nd_2O_3$ compared to growth with $NdCl_3$, local alignment of each gene, and HMM prediction of the gene products of the cluster. *q* values represent false discovery rate-adjusted *p* values. *B*) The META1p4129 through META1p4138 cluster shares high percent amino acid identity with BGCs in other methylotrophs and proteobacteria but shares no similarity with the aerobactin BGC of *G. hollisae.*

***The LCC produces a siderophore-like compound, a novel lanthanophore.*** Phyre2 modeling suggests some gene products of the LCC resemble those for aerobactin biosynthesis. Thus, we investigated the binding of aerobactin to Ln. Using an indirect dye-based assay with the triphenylmethane dye chrome azurol S (CAS) and the cationic surfactant hexadecyltrimethylammonium bromide (HDTMA), we obtained qualitative measurements of the ability of aerobactin to bind Nd, La and lutetium (Lu) across pH conditions. The assay is based on the findings of Gladilovich and Kuban who used CAS/HDTMA for the determination of $Ln^{3+}$ and yttrium $(Y)^{3+}$ concentrations (39, 40) and inspired by the commonly known CAS assay for the detection of siderophores (41). These assays showed that at physiological pH aerobactin was able to bind Nd, La, and lutetium (Lu) and that the Ln binding efficiency of aerobactin is affected by pH (Fig. 3*A* and Fig. S2). The higher the pH of the solution, the stronger the initial interaction with CAS/HDTMA and the more effective aerobactin was in binding the Ln. Interestingly, differences in the binding capacities with different Ln was observed, as three equivalents of aerobactin were enough to completely displace Lu from CAS/HDTMA at pH 8, but not La or Nd (Fig. S2).

Because aerobactin can bind Nd at physiological pH, we determined the effect of adding exogenous aerobactin in our growth conditions. When methanol growth was dependent on Ln-dependent machinery including XoxF and ExaF, addition of aerobactin to the growth media had no significant effect on growth rate or growth yield when using $Nd_2O_3$ or $NdCl_3$ (Fig 3*B*).

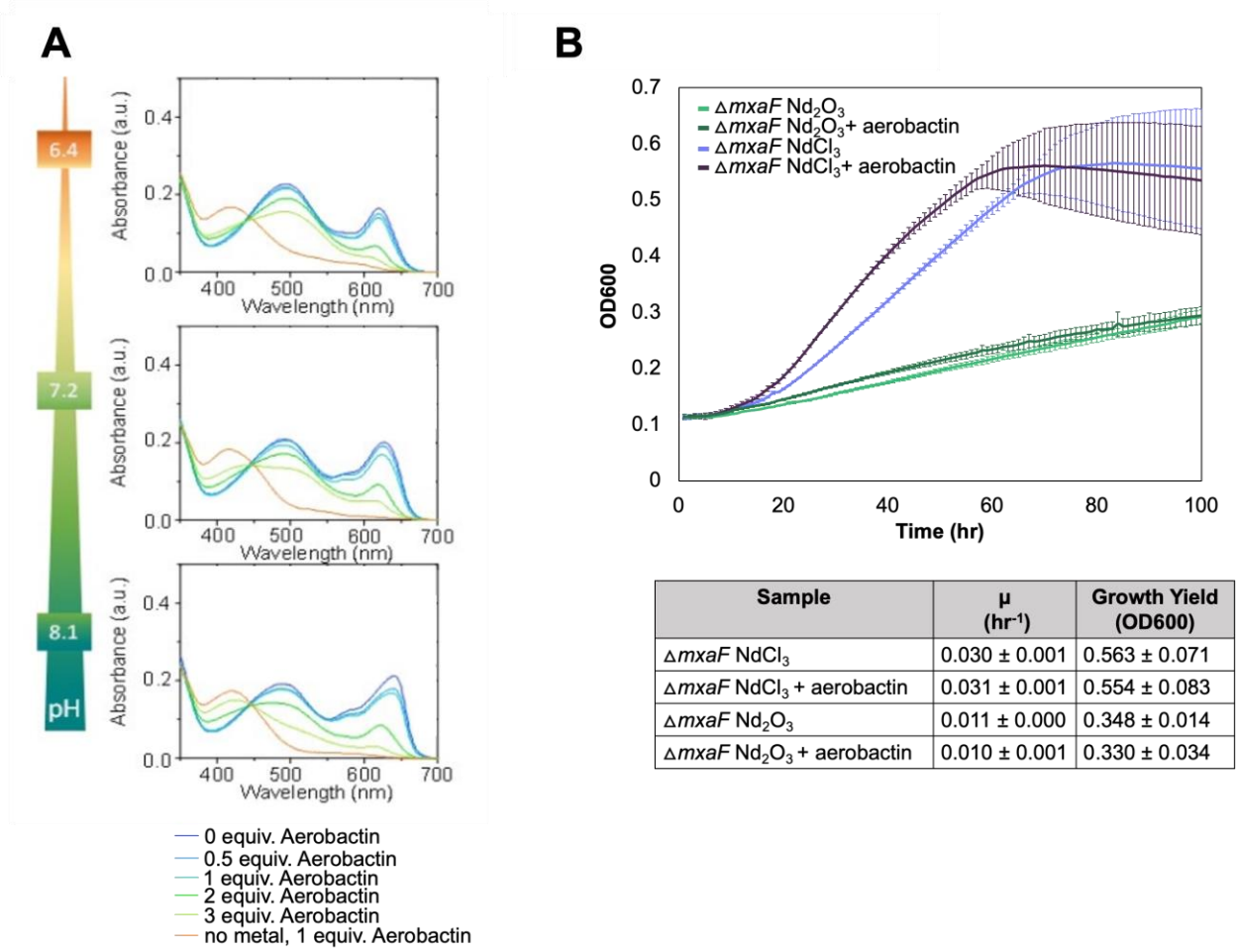


| Sample | μ ($hr^{-1}$) | Growth Yield (OD600) |
|---|---|---|
| Δ*mxaF* $NdCl_3$ | 0.030 ± 0.001 | 0.563 ± 0.071 |
| Δ*mxaF* $NdCl_3$ + aerobactin | 0.031 ± 0.001 | 0.554 ± 0.083 |
| Δ*mxaF* $Nd_2O_3$ | 0.011 ± 0.000 | 0.348 ± 0.014 |
| Δ*mxaF* $Nd_2O_3$ + aerobactin | 0.010 ± 0.001 | 0.330 ± 0.034 |

**Figure 3. Characterization of aerobactin as a Ln-chelator *in vitro* and *in vivo*.** *A*) CAS/HDTMA assay with aerobactin at three different pH values (6.4, 7.2, 8.1) in MOPSO/HEPES buffer (1.5 mM/1.5 mM) with $NdCl_3$. The concentrations of buffer, metal (18.75 μM), and CAS/HDTMA (18.75 μM/50 μM) were kept constant while the concentration of aerobactin varied from 0 μM to 56.25 μM. *B*) Effect of 2 μM aerobactin on growth of Δ*mxaF* with $NdCl_3$ or $Nd_2O_3$. Individual data points represent the mean of three replicates. Aerobactin does not significantly affect growth rate (*p* values > 0.05) or growth yield (*p* values > 0.05) of Δ*mxaF* with either $NdCl_3$ or $Nd_2O_3$.

***Expression of the LCC* in trans *enables secretion of a compound that improves Ln-dependent growth.*** A plasmid containing the putative biosynthetic genes of the LCC, META1p4132 through META1p4138, was constructed via the DNA assembler method developed by Shao et al. (42) (Fig. 4*A*). This plasmid was transformed into an Δ*mxaF* background, generating Δ*mxaF*/pAZ001. To determine if the product of the LCC is secreted, Δ*mxaF*/pAZ001 was grown with $Nd_2O_3$ to an OD600 of 0.3, after which the supernatant was collected, filter sterilized, and used to resuspend Δ*mxaF* cells grown with $Nd_2O_3$. Growth of this manipulated culture was compared to a Δ*mxaF* culture grown in methanol with $Nd_2O_3$ that had been resuspended in its own supernatant. Exchange with the Δ*mxaF*/pAZ001 supernatant increased Δ*mxaF* growth by over 40% (Fig. 4*B*). Furthermore, expression of this cluster *in trans* improved the growth on $Nd_2O_3$, increasing growth rate by 47% and growth yield by 20%. Conversely, growth on $NdCl_3$ was diminished, with growth rate and yield decreasing by 42% and 44%, respectively (Fig. 4*CD*).

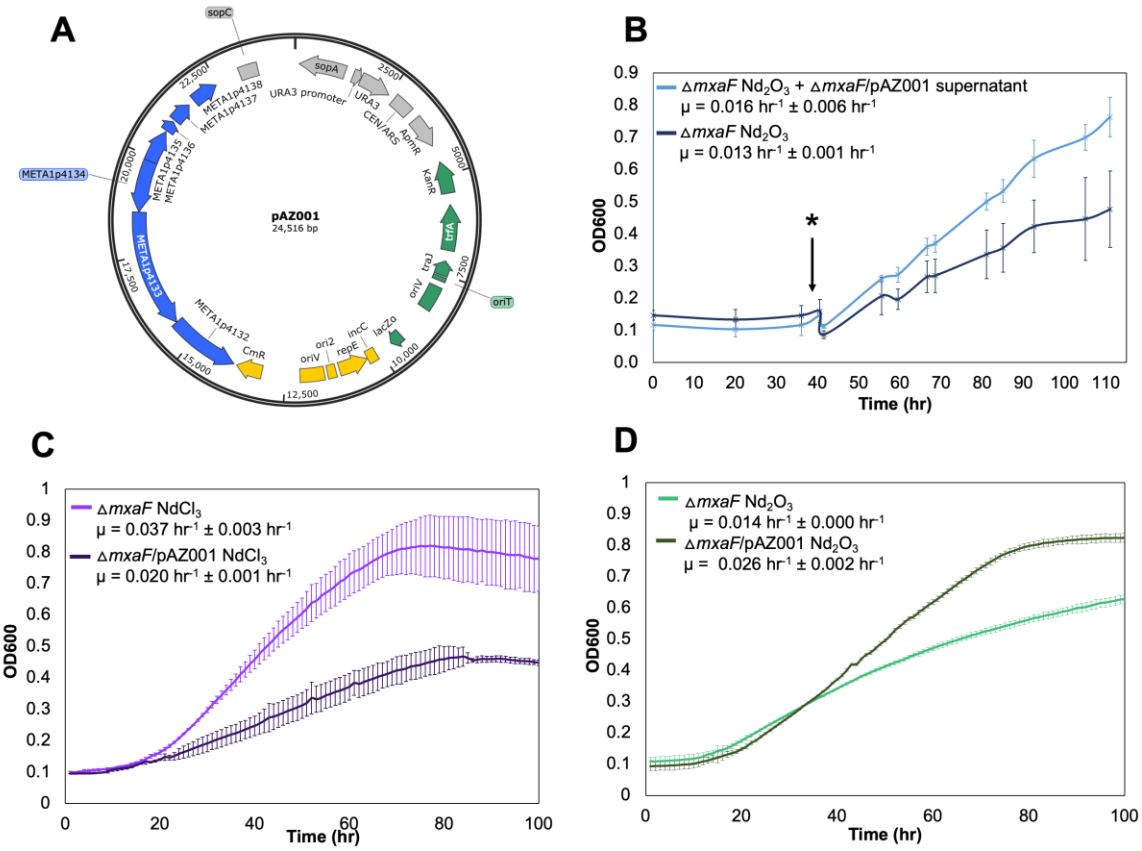


**Figure 4. Effect of expression of LCC *in trans* during Ln-dependent growth.** *A*) Plasmid map of pAZ001 with META1p4129 through META1p4138 (blue) and segments for expression in *S. cerevisiae* (grey), *M. extorquens* (green), and *E. coli* (yellow). *B*) Growth rate of Δ*mxaF* is significantly increased (*p* value < 0.05) during growth with $Nd_2O_3$ when its supernatant is replaced with supernatant from Δ*mxaF*/pAZ001 (light blue) compared to a control that was resuspended in its own supernatant (dark blue). Asterisk and arrow denote the time at which supernatants were manipulated. *C*) Growth rate of Δ*mxaF*/pAZ001 (dark purple) is significantly decreased (*p* value < 0.005) during growth on $NdCl_3$ compared to Δ*mxaF* (light purple). *D*) Growth rate of Δ*mxaF*/pAZ001 (light green) is significantly increased (*p* value < 0.005) during growth on $Nd_2O_3$ compared to Δ*mxaF* (dark green). Individual data points represent the mean of three replicates.

***LCC expression* in trans *increases Ln accumulation from the low-grade Ln-source NdFeB magnet swarf.*** Ln bioaccumulation was measured via ICP-MS of Δ*mxaF* and Δ*mxaF*/pAZ001 cell pellets from cultures grown in methanol minimal medium with either $Nd_2O_3$, $NdCl_3$, or 1% pulp density NdFeB magnet swarf. NdFeB magnet swarf is a complex, insoluble Ln source that has commercial value for Ln recovery. Expression of the LCC *in trans* significantly increased $Nd^{3+}$ bioaccumulation during growth with the insoluble sources $Nd_2O_3$ (2.3-fold) and magnet swarf (3.2-fold). NdFeB magnet swarf also contains significant amounts of the light Ln $Pr^{3+}$ and the heavy Ln $Dy^{3+}$, both of which have high technological value. Bioaccumulation of these Lns was increased on average by 3.5-fold with expression of the LCC *in trans* (Fig. 5*A*). Despite these effects with insoluble sources, expression of the LCC did not significantly increase $Nd^{3+}$ with the soluble source $NdCl_3$ (Fig. 5*A*). Finally, we probed the specificity of the LCC-generated lanthanophore by measuring $Fe^{3+}$ content in the same cells. Expression of the LCC *in trans* resulted in no significant differences in $Fe^{3+}$ bioaccumulation between Δ*mxaF* and Δ*mxaF*/pAZ001 when using pure Ln sources but there was a significant difference in $Fe^{3+}$ bioaccumulation of 1.4-fold when using magnet swarf (Fig. 5*B*).

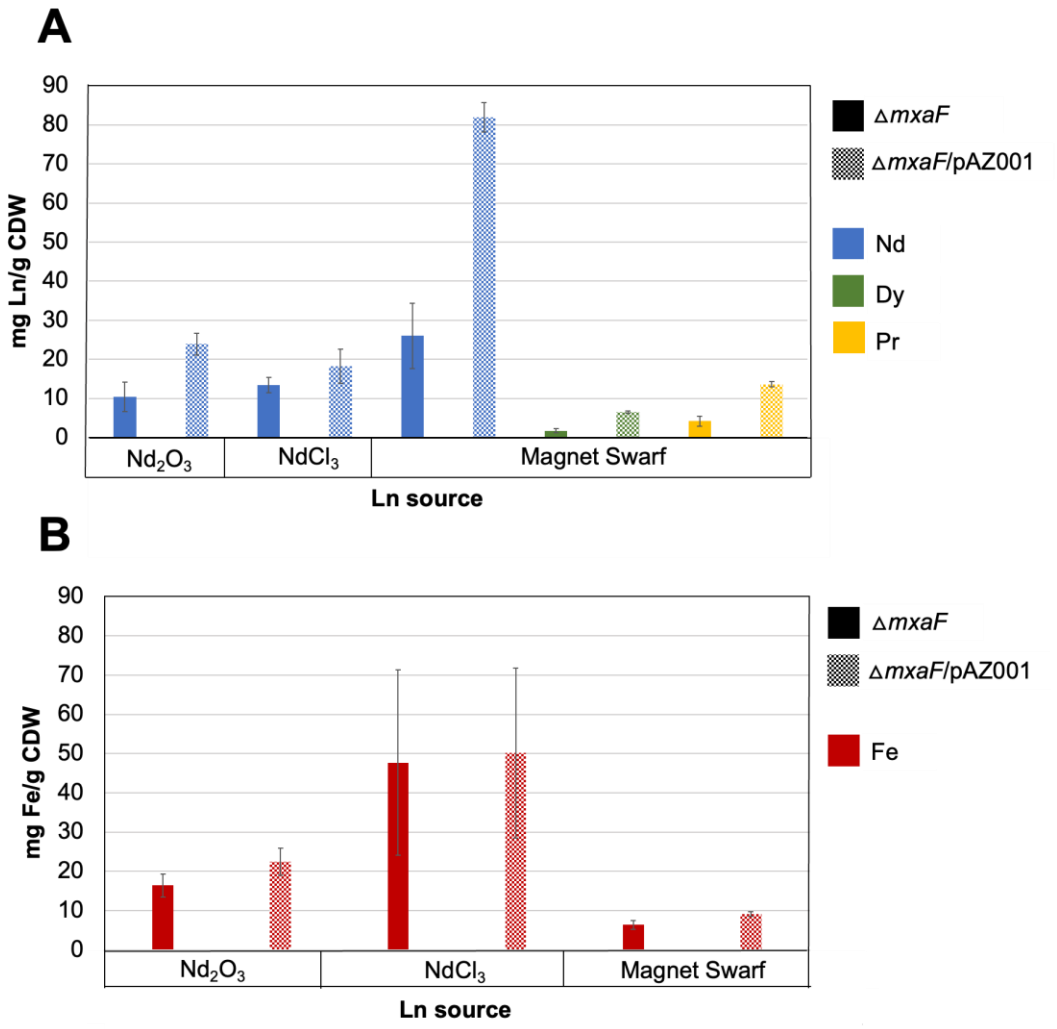


**Figure 5. LCC product increases Ln bioaccumulation in *M. extorquens*.** Bioaccumulation of Ln and $Fe^{3+}$ in Δ*mxaF* (solid bars) and Δ*mxaF*/pAZ001 (checkered bars) cell pellets as quantified by ICP-MS. Values represent the mean of three replicates. *A*) Δ*mxaF*/pAZ001 shows significantly increased bioaccumulation of $Nd^{3+}$ (blue) with $Nd_2O_3$ (*p* values < 0.05) and magnet swarf (*p* value < 0.0005), but not with $NdCl_3$ (*p* value > 0.05). Δ*mxaF*/pAZ001 also shows significantly increased bioaccumulation of the heavy Ln $Dy^{3+}$ (green) and the light Ln $Pr^{3+}$ (yellow) with magnet swarf as a Ln source (*p* values < 0.0005). *B*) Δ*mxaF*/pAZ001 does not

significantly increase the bioaccumulation of $Fe^{3+}$ (red) when grown with $Nd_2O_3$ or $NdCl_3$ ($p$ values > 0.05) but does with magnet swarf ($p$ value < 0.0005)

## DISCUSSION

Ln, along with scandium and yttrium, are a group of chemically and physically similar elements known as "Rare Earth Elements" (REEs). REEs were named as such due to their insolubility and the lack of their presence in concentrated mineral deposits and rich ores. Despite their name, total concentrations of REE in the Earth's crust are similar to those of copper, zinc, and lead (43–45) and together these metals comprise about 0.015% of the total material in the Earth's crust (46). REE are most frequently found in highly insoluble phosphate and oxide mineral forms, restricting bioavailability (28). Though the number of studies investigating various aspects of REE biochemistry, including Ln metabolism in bacteria, have increased considerably over the past decade, nearly all of these studies have used soluble Ln chloride salts as a REE source. Therefore, it is important to understand how solubility and bioavailability of REE impact the metabolism and physiology of organisms that use these metals. Here, we leveraged RNAseq transcriptomics to measure changes in gene expression that could indicate REE uptake mechanisms related to REE bioavailability and identified the LCC: the first reported BGC encoding a secreted Ln-chelating molecule, a lanthanophore.

We surveyed the RefSeq non-redundant protein record for organisms that encode clusters similar in identity to the LCC, META1p4129 through META1p4138, and found that the LCC is conserved across methylotrophs from diverse environments such as the phyllosphere, drinking water, and the human oral cavity (Fig. 2*B*). The LCC is also present in *Beijerinckiaceae indica* ATCC9039, which is closely related to methanotrophs and methylotrophs, but is itself a

generalist (47). *B. indica* ATCC9039 was isolated from rice paddies, an environment with poorly bioavailable Lns. The genome of the thermoacidophilic methanotroph *Methylacidiphilum fumariolicum* SolV does not contain the LCC genes; as SolV resides in an extreme environment where Ln are more bioavailable, it would not require the LCC product to solubilize Ln. Corroborating its presence in organisms that need to solubilize Ln in their environments and its absence in organisms that already have soluble Ln available in their environments, we found the LCC to be highly upregulated in response to poorly soluble Ln compared to soluble Ln (Fig. 2*A*).

To further investigate the role of the LCC product in modulating Ln bioavailability, we aimed to generate a strain that expressed the LCC *in trans*. The size (9 kb) and GC content (> 70%) of the LCC made cloning using standard methods arduous, so the DNA assembler method of Shao et al. was implemented to generate pAZ001 (Fig 4*A*). Developed as a tool to facilitate the study of large, cryptic, or otherwise inaccessible natural product BGCs, DNA assembler has been used to express complete opioid biosynthesis pathways in yeast and to discover novel polycyclic tetramate macrolactams in *S. griseus* (48, 49). DNA assembler leverages *S. cerevisiae in vivo* homologous recombination for assembly of constructs and *E. coli* for plasmid enrichment. After purification of pAZ001, we were able to generate Δ*mxaF*/pAZ001, which exhibited improved growth on $Nd_2O_3$ (Fig. 4*D*).

The first biosynthetic gene of the LCC, META1p4132, shows homology to aerobactin synthetase *iucA*, which catalyzes the condensation of citrate and *N*6-acetyl-*N*6-hydroxy-L-lysine (Fig. 2*B*). IucA has been shown to be incredibly specific for its substrate, citrate, with a $K_M$ of 180 μM (50). As META1p4132 seems to be a homolog of *iucA*, it is plausible that the starting point for lanthanophore biosynthesis is citrate. Due to this similarity between the LCC and the aerobactin biosynthetic gene cluster, we tested the ability of the citrate-derived siderophore aerobactin to

bind Ln. Using an indirect dye-based assay containing CAS, HDTMA and $LnCl_3$ it was shown that aerobactin binds light and heavy Ln at physiological pH. The free CAS dye absorption is around 410 nm and the Nd-CAS complex absorbs under the chosen conditions with maxima at 495 and 625 nm. The higher the pH, the more effective aerobactin is in binding the Ln (Fig. 3*A*, S1). The pH-dependence of aerobactin-Ln binding could point towards a possible mechanism of Ln release in the cell by the lanthanophore. While a reduction to enable decomplexation (as in the case of iron-siderophore complexes (51) is not feasible for Ln, a local pH change could facilitate the Ln release from a lanthanophore. Despite the result that aerobactin can bind Nd, addition of aerobactin equimolar to Nd was not shown to have any effect on the growth rate or yield of Δ*mxaF* grown with $NdCl_3$ or $Nd_2O_3$ (Fig. 3*B*). Additionally, *M. extorquens* AM1 lacks homologs to the remaining genes necessary for aerobactin synthesis (*iucB, iucC,* and *iucD)* (Fig. 2*C*). While results indicate that the LCC does not produce aerobactin, they do not preclude that it may encode for another siderophore, possibly with a similar structural motif.

We determined if expression of LCC *in trans* increased intracellular Ln and Fe concentrations. In Δ*mxaF*/pAZ001 Nd accumulation from poorly soluble Ln sources increased significantly when compared to *mxaF*. However, Nd accumulation did not increase when using $NdCl_3$, presumably because Ln chlorides are already soluble (Fig. 5*A*). Interestingly, expression of the LCC *in trans* also increased bioaccumulation of the light Ln Pr and the heavy Ln Dy when using magnet swarf. Increased bioaccumulation of Fe occurred only when using magnet swarf (Fig. 5*B*) and could be due to leaching excess Fe from the magnet and unspecific binding from the lanthanophore (Fig. S3). Taken together, we propose that the LCC products does not produce a siderophore but instead produces a novel metallophore with a preference for binding Ln, thus a lanthanophore. While the structure of the lanthanophore remains under investigation, it is

exciting to postulte that the molecule could be engineered to bind specific Ln, which would expand current techniues for Ln separation and minining.

The similarities between the LCC and siderophore biosynthetic gene clusters make the known siderophore uptake mechanisms useful scaffolds for understanding the potential secretion and uptake of the lanthanophore. Siderophores must interact with insoluble Fe compounds in the environment, so we investigated whether the LCC product is similarly secreted. While growing Δ*mxaF* with $Nd_2O_3$, we found that replacing the Δ*mxaF* supernatant with Δ*mxaF*/pAZ001 supernatant significantly increased the growth rate of Δ*mxaF*, confirming that the lanthanophore is secreted (Fig 3*B*). Interestingly, the LCC encodes for a TonB-receptor (META1p4129) and it is possible that this receptor facilitates the transport of a Ln-lanthanophore complex into the periplasm. An attractive candidate for an additional Ln-lanthanophore uptake system is the *lut* cluster, which is shown in this study to be differentially co-expressed with the LCC during growth with $Nd_2O_3$ (Fig 1*C*). Furthermore, the *lut* cluster contains analogous components of siderophore-iron uptake systems, namely a TonB-dependent transporter (*lutH*) and an ABC transport system (*lutA*, *lutE*, *lutF*), which have been shown to be necessary for Ln-dependent growth and transport of Ln into the cytoplasm when using soluble Ln sources (25). The presence of an active transport system for lanthanophore bound Nd, separate from import via ion channels, could increase periplasmic levels of Nd and increase growth rate through increasing Ln-dependent ADH activity. Conversely, importing an excess of lanthanophore bound Nd could negatively affect the cell through metal toxicity, which could explain why Δ*mxaF*/pAZ001 shows a decreased growth rate with $NdCl_3$ compared to Δ*mxaF* (Fig. 3*C*).

It has been suggested that Ln are made available in the periplasm for coordination with XoxF-type MDHs and ExaF EtDH, all of which are periplasmic enzymes. These proteins have Sec

pathway signal peptides, indicating that they are translocated unfolded from the cytoplasm to the periplasm where they attain their folded conformation. However, to date there is no empirical evidence that XoxF or ExaF bind Ln in the periplasm. If the lanthanophore functions similarly to siderophores that release Fe in the cytoplasm (52), it is possible that Ln are not made bioavailable until they are released from their chelator in the cytoplasm. It has already been shown in *M. extorquens* that Ln must be transported to the cytoplasm for growth dependent on XoxF MDH, as deletion of the ABC transporter components *lutE* and *lutF* causes accumulation of Ln in the periplasm and a lack of growth (25, 26). It is currently not entirely understood if this requirement is transcriptional, as the presence of Ln at sub-micromolar concentrations effects a switch from MxaFI to XoxF MDH (32), or if essential Ln-dependent cytoplasmic enzymes remain to be discovered. We recently reported the discovery of the lanthasome, a Ln-polyphosphate granule containing microcompartment in *M. extorquens* AM1, that resembles an acidocalcisome (31). As pH change is a likely mechanism for dissociation of the Ln from the lanthanophore, the necessity for Ln to be transported to the cytoplasm could be explained through the lanthasome serving as a localized storage and decoupling compartment. It is possible that after separation from the lanthanophore, cytoplasmic Ln are transported back out to the periplasm for coordination with XoxF-type MDHs or ExaF EtDH.

We also observed that decreased Ln solubility results in upregulation of the alternative methanol oxidation system encoded by *exaF* (Fig. 1*C*). The importance of ExaF has already been noted for its ability to use the heavy Ln $Gd^{3+}$ in the enzyme cofactor complex (31).

Previous work has shown extracts of a *M. extorquens* strain evolved to use the heavy Ln Gd have exhibited a 6-fold increase in PQQ levels compared to Δ*mxaF* extracts (32). This result suggests that PQQ might facilitate Ln bioavailability, yet here we did not observe an increase in

the expression of most PQQ biosynthetic genes during growth with poorly bioavailable $Nd_2O_3$. However, increased expression of two orphan *pqqA* genes was observed (Fig. 1*C*). *pqqA*, encoding the peptide precursor to PQQ, has previously been reported to be nonessential for PQQ biosynthesis in *M. extorquens* AM1, but orphan *pqqA* copies were not investigated in these studies (29). In *Methylovorus* sp. MP688, which is equipped with five *pqqA* copies, the availability of PqqA has been shown to be a rate determining step in PQQ biosynthesis (53). Taken together with our results, it is possible that PqqA could play a regulatory role in the response of *M. extorquens* AM1 to Ln solubility.

## METHODS

### Strains and cultivation

*M. extorquens* AM1 strains (WT $Rif^R$ derivative (54), Δ*mxaF* (55), and Δ*mxaF*/pAZ001) were grown in Hypho medium (56) but reducing the phosphate concentration to 8.32 mM. 3 mL cultures with 15 mM succinate (MilliporeSigma, Burlington, MA, USA) were grown overnight in round-bottom glass culture tubes (Thermo Fisher Scientific, Waltham, MA, USA) at 30 °C, shaking at 200 rpm on an Innova S44i shaker (Eppendorf, Hamburg, Germany) and subcultured into fresh media containing 50 mM methanol. Trace metals grade $Nd_2O_3$ and $NdCl_3$ (MilliporeSigma, Burlington, MA, USA) were added to final neodymium concentrations of 2 μM unless otherwise indicated. NdFeB magnet swarf (Urban Mining Company, San Marcos, TX, USA) was added to a final pulp density of 1%. YPAD medium containing 1% yeast extract, 2% peptone, and 2% dextrose supplied with 0.01% adenine hemisulphate was used to grow *S. cerevisiae* HZ848 (*MATα ade2-1 ade3*Δ*22* Δ*ura3 his3-11,15 trp1-1 leu2- 3,112 can1-100*) at 30 °C, shaking at 250 rpm on an Innova S44i shaker (Eppendorf, Hamburg, Germany). Yeast

transformants were maintained on synthetic complete drop-out medium lacking uracil (MilliporeSigma, Burlington, MA). TransforMAX EPI300 *E. coli* (Lucigen, Middleton, WI) were grown on SOB medium at 37 °C, shaking at 250 rpm on an Innova S44i shaker (Eppendorf, Hamburg, Germany). *E. coli* transformants were maintained on Lysogeny Broth medium (57) (BD, Franklin Lakes, NJ). *E. coli* were induced to express pAZ001 using CopyControl Induction Solution (Lucigen, Middleton, WI, USA). When necessary, kanamycin, chloramphenicol, ampicillin, and aerobactin were added to final concentrations of 50 μg/mL, 12.5 μg/mL, 50 μg/mL, and 2 μM, respectively. Growth curves were obtained with 650 μL cultures grown in transparent 48 well plates (Corning, Corning, NY, USA) incubated at 30 °C, shaking at 548 rpm using a Synergy HTX plate reader (BioTek, Winooski, VT, USA).

RNA-seq transcriptomics

50 mL cultures were grown in 250 mL glass Erlenmeyer flasks to an OD600 of 0.8, which corresponded to mid-exponential growth. Cultures that did not require the addition of Ln were grown in glassware that had not been exposed to Ln, while cultures that required the addition of Ln were grown in glassware that had only been exposed to the Ln that was to be added to the medium. Total RNA samples were generated, and quality was corroborated as described previously (58). rRNA depletion using the Ribo-Zero RNA Plus rRNA Depletion Kit (Illumina, San Diego, CA, USA), library preparation, and Illumina Hi-Seq sequencing were performed by the Microbial Genome Sequencing Center (MiGS, Pittsburgh, PA, USA). Using KBase (59), reads were aligned with HISTAT2, transcripts were assembled with StringTie, and DEGs were identified using DESeq2. The RNA-seq transcriptomics datasets generated and analyzed during this study are available in Table S3.

DNA manipulation

To prepare plasmid pAZ001, a yeast *in vivo* DNA assembly strategy was used based on the DNA assembler method (42). Primers used to construct fragments can be found in Table S2. First, the genes META1p4132 through META1p4133 and META1p4134 through META1p4138 were PCR-amplified as two 4.5 kb fragments with 400 bp of overlap on each end from *M. extorquens* AM1 gDNA isolated using the DNeasy PowerMax Soil Kit (Qiagen, Germantown, MD, USA). Two expression elements were obtained using pRES (unpublished) as template: a 4.0 kb *E. coli* helper fragment (derived from pCC1Fos (Genbank accession EU140751, Epicentre Biotechnologies, Madison, WI, USA) and a 3.3 kb *S. cerevisiae* helper fragment (derived from pYJKSD,(60)). A third fragment (5.0 kb) to integrate elements of expression for *M. extorquens* AM1 was obtained by using pCM66T as a template. To prevent competition with the *E. coli* backbone, the *colE* locus of pCM66T was removed with OE-PCR through amplification of the components up and downstream of *colE* locus. Four different 800 bp joint fragments with 400 bp overlaps with each main fragment were obtained by amplifying expression elements from the *E. coli* fragment, the *S. cerevisiae* fragment, the LCC gene fragments, and the *M. extorquens* AM1 fragment. Following electrophoresis, PCR products were purified from a 1% agarose gel using the GeneJET Gel Extraction Kit (Thermo Fisher Scientific, Waltham, MA, USA). 150 ng of each PCR product was combined, dried under $N_2$, and the final mixture was resuspended in 4 µL of Milli-Q double deionized water. Electrocompetent, uracil auxotrophic *S. cerevisiae* HZ848 were freshly prepared and transformed with this mixture and spread on synthetic complete medium minus uracil (SC-ura) plates to select for homologous recombination of the DNA mixture. Eight prototrophic colonies were grown in liquid SC-ura and lysed using the Zymoprep Yeast Plasmid MiniPrep II Kit (Zymo Research, Irvine, CA, USA). The plasmid was purified

from lysate using the Zymo Research BAC DNA Miniprep Kit (Zymo Research, Irvine, CA, USA) according to the manufacturer's protocol. The plasmid was then transformed into electrocompetent TransforMax EPI300TM *E. coli* (Lucigen, Middleton, WI, USA), and plated on LB with chloramphenicol for selection. Resultant colonies were grown in liquid SOB media overnight followed by induction through passaging into fresh media with chloramphenicol and CopyControl Induction Solution (Lucigen, Middleton, WI, USA). After five hours of growth, the plasmid was purified using BAC DNA Miniprep Kit (Zymo Research, Irvine, CA) and verified via Sanger sequencing (UC Berkeley DNA Sequencing Facility, Berkeley, CA, USA). The plasmid was then used in the electroporation of Δ*mxaF* to generate strain Δ*mxaF*/pAZ001.

Secretion of LCC product bioassay

3 mL cultures of Δ*mxaF* and Δ*mxaF*/pAZ001 were grown for 40 hours and spun down at 2000xg to collect supernatants. Both supernatants were sterilized by filtration (0.22 μm polyethersulfone, VWR, Radnor, PA, USA). The Δ*mxaF* control condition was resuspended in its own supernatant, while the Δ*mxaF* test condition was resuspended in Δ*mxaF*/pAZ001 supernatant. Growth was monitored by measuring optical density (OD600) over 70 hours.

Chrome Azurol S (CAS) Assay for Spectrophotometric Determination of Ln-binding Ligands

All solutions used for the assay described herein were prepared in ultrapure water (type 1, pH 5.5; Synergy® UV system from Merck Millipore®, Darmstadt, Germany). Chrome azurol S (Sigma-Aldrich, Burlington, MA, USA), Hexadecyltrimethylammonium bromide (HDTMA, >99%, ACROS Organics, Geel, Belgium), $LaCl_3$ x 7 $H_2O$ (99.999%, Sigma Aldrich, St Louis, MO, USA), $NdCl_3$ x 6 $H_2O$ (99.9%, abcr, Karlsruhe, Germany) and $LuCl_3$ x 6 $H_2O$ (99.999%, Sigma Aldrich, St Louis, MO, USA) were commercially obtained and used without further purification. pH

measurements were carried out with a FiveEasy pH-meter (Mettler Toledo, Greifensee, Switzerland) which was calibrated prior to use. The assay was performed in transparent 96-well-plates (Corning, Corning, NY, USA) using an epoch2 plate reader (BioTek, Winooski, VT, USA). Data was pathlength and baseline corrected using the software Gen5 3.03 and plotted with Origin(Pro), Version *2018* (OriginLab Corporation, Northampton, MA, USA). Stock solutions were freshly prepared. 0.25 mM metal solutions ($LaCl_3$ x 7 $H_2O$, $NdCl_3$ x 6 $H_2O$, $LuCl_3$ x 6 $H_2O$) were prepared from 10 mM stock solutions in water which had been stored in aliquots at −25 °C. Aerobactin was prepared as 0.25 mM solution in water. Final concentrations of MOPSO/HEPES buffer (1.5 mM/1.5 mM), CAS (18.75 µM), HDTMA (50 µM), and metal (18.75 µM) were kept constant while the concentration of aerobactin (0 µM – 56.25 µM) was varied. pH values of buffer were adjusted to 6.4, 7.2, and 8.1 with NaOH (6 M) before the solutions were made up to the final volume. The final volume in each well was 200 µL. The reagents were added in the following order: water, buffer, CAS/HDTMA Assay-Mix, metal solution, aerobactin. The plate was then incubated for 5 minutes at room temperature (180 cpm, orbital shake). The UV-Vis spectra were recorded in the range from 350 nm to 750 nm in 1 nm intervals with a scan rate of 8 measurements per data point.

Aerobactin synthesis

Aerobactin was synthesized in six steps with modifications after published procedures (61, 62) starting from commercially available Cbz-Lys(Boc)-OH. Experimental details and characterization can be found in the Supporting Information.

Elemental analysis of culture pellets

50 mL cultures were grown in 250 mL erlenmeyer flasks to OD600 ranging from 0.2 to 0.4. Cells were pelleted at 4000 x g and pellets were washed three times with 10 mL of milliQ $H_2O$ and resuspended in 1 mL of milliQ $H_2O$. 1 mL of TraceMetal Grade 70% $HNO_3$ (Thermo Fisher Scientific, Waltham, MA) was then added to resuspended cell pellets. Acidified cell pellets were boiled at 90 °C for 1 hour and then pelleted at 4000 x g. 1 mL of each sample was then diluted with 19 mL of milliQ $H_2O$. Samples were analyzed via ICP-MS (Laboratory for Environmental Analysis, Athens, GA, USA).

## FUNDING

The information, data, or work presented herein was funded in part by the Advanced Research Projects Agency-Energy, U.S. Department of Energy, under Award Number DE-AR0001337. The views and opinions of authors expressed herein do not necessarily state or reflect those of the United States Government or any agency thereof. This material is also based upon work supported by the National Science Foundation under Grants 2127732. LJD gratefully acknowledges the ERC Starting grant Lanthanophor (945846).

## ACKNOWLEDGEMENTS

We thank Richard Ngo for his guidance in the use of cblaster.

## REFERENCES

1. E. I. Solomon, U. M. Sundaram, T. E. Machonkin, Multicopper Oxidases and Oxygenases. *Chem. Rev.* **96**, 2563–2606 (1996).

2. C. Andreini, I. Bertini, G. Cavallaro, G. L. Holliday, J. M. Thornton, Metal ions in biological catalysis: from enzyme databases to general principles. *J. Biol. Inorg. Chem.* **13**, 1205–1218 (2008).

3. K. J. Waldron, J. C. Rutherford, D. Ford, N. J. Robinson, Metalloproteins and metal

sensing. *Nature* **460**, 823–830 (2009).

4. J. Morrissey, M. L. Guerinot, Iron uptake and transport in plants: the good, the bad, and the ionome. *Chem. Rev.* **109**, 4553–4567 (2009).

5. J. Kramer, Ö. Özkaya, R. Kümmerli, Bacterial siderophores in community and host interactions. *Nat. Rev. Microbiol.* **18**, 152–163 (2020).

6. S. Gama, *et al.*, Iron Coordination Properties of Gramibactin as Model for the New Class of Diazeniumdiolate Based Siderophores. *Chemistry* **27**, 2724–2733 (2021).

7. K. D. Krewulak, H. J. Vogel, Structural biology of bacterial iron uptake. *Biochim. Biophys. Acta* **1778**, 1781–1804 (2008).

8. F. Imperi, F. Tiburzi, P. Visca, Molecular basis of pyoverdine siderophore recycling in Pseudomonas aeruginosa. *Proc. Natl. Acad. Sci. U. S. A.* **106**, 20440–20445 (2009).

9. W. Neumann, M. Sassone-Corsi, M. Raffatellu, E. M. Nolan, Esterase-Catalyzed Siderophore Hydrolysis Activates an Enterobactin-Ciprofloxacin Conjugate and Confers Targeted Antibacterial Activity. *J. Am. Chem. Soc.* **140**, 5193–5201 (2018).

10. A. Pol, *et al.*, Rare earth metals are essential for methanotrophic life in volcanic mudpots. *Environ. Microbiol.* **16**, 255–264 (2014).

11. J. T. Keltjens, A. Pol, J. Reimann, H. J. M. Op den Camp, PQQ-dependent methanol dehydrogenases: rare-earth elements make a difference. *Appl. Microbiol. Biotechnol.* **98**, 6163–6183 (2014).

12. L. Chistoserdova, Lanthanides: New life metals? *World J. Microbiol. Biotechnol.* **32**, 138 (2016).

13. G. Tircsó, *et al.*, Lanthanide(III) complexes of some natural siderophores: a thermodynamic, kinetic and relaxometric study. *J. Inorg. Biochem.* **127**, 53–61 (2013).

14. B. E. Allred, *et al.*, Siderocalin-mediated recognition, sensitization, and cellular uptake of actinides. *Proc. Natl. Acad. Sci. U. S. A.* **112**, 10342–10347 (2015).

15. L. J. Daumann, P. Werther, M. J. Ziegler, K. N. Raymond, Siderophore inspired tetra- and octadentate antenna ligands for luminescent Eu(III) and Tb(III) complexes. *J. Inorg. Biochem.* **162**, 263–273 (2016).

16. B. Jahn, *et al.*, Similar but Not the Same: First Kinetic and Structural Analyses of a Methanol Dehydrogenase Containing a Europium Ion in the Active Site. *Chembiochem* (2018) https:/doi.org/10.1002/cbic.201800130.

17. N. M. Good, *et al.*, Lanthanide-dependent alcohol dehydrogenases require an essential aspartate residue for metal coordination and enzymatic function. *J. Biol. Chem.* **295**, 8272–8284 (2020).

18. K. Takeda, *et al.*, Characterization of a novel PQQ-dependent quinohemoprotein pyranose dehydrogenase from Coprinopsis cinerea classified into auxiliary activities family 12 in carbohydrate-active enzymes. *PLoS One* **10**, e0115722 (2015).

19. H. Matsumura, *et al.*, Discovery of a eukaryotic pyrroloquinoline quinone-dependent oxidoreductase belonging to a new auxiliary activity family in the database of carbohydrate-active enzymes. *PLoS One* **9**, e104851 (2014).

20. L. Chistoserdova, Modularity of methylotrophy, revisited. *Environ. Microbiol.* **13**, 2603–2622 (2011).

21. N. M. Good, *et al.*, Pyrroloquinoline Quinone Ethanol Dehydrogenase in Methylobacterium extorquens AM1 Extends Lanthanide-Dependent Metabolism to Multicarbon Substrates. *J. Bacteriol.* **198**, 3109–3118 (2016).

22. L. Wang, *et al.*, Lanthanide-dependent methanol dehydrogenase from the legume symbiotic nitrogen-fixing bacterium Bradyrhizobium diazoefficiens strain USDA110. *Enzyme Microb. Technol.* **130**, 109371 (2019).

23. C.-E. Wegner, L. Gorniak, S. Riedel, M. Westermann, K. Küsel, Lanthanide-Dependent Methylotrophs of the Family Beijerinckiaceae: Physiological and Genomic Insights. *Appl. Environ. Microbiol.* **86**, 1–18 (2019).

24. M. Wehrmann, P. Billard, A. Martin-Meriadec, A. Zegeye, J. Klebensberger, Functional Role of Lanthanides in Enzymatic Activity and Transcriptional Regulation of Pyrroloquinoline Quinone-Dependent Alcohol Dehydrogenases in Pseudomonas putida KT2440. *MBio* **8**, e00570–17 (2017).

25. P. Roszczenko-Jasińska, *et al.*, Gene products and processes contributing to lanthanide homeostasis and methanol metabolism in Methylorubrum extorquens AM1. *Sci. Rep.* **10**, 12663 (2020).

26. A. M. Ochsner, *et al.*, Use of rare-earth elements in the phyllosphere colonizer Methylobacterium extorquens PA1. *Mol. Microbiol.* **111**, 1152–1166 (2019).

27. N. C. Martinez-Gomez, H. N. Vu, E. Skovran, Lanthanide Chemistry: From Coordination in Chemical Complexes Shaping Our Technology to Coordination in Enzymes Shaping Bacterial Metabolism. *Inorg. Chem.* **55**, 10083–10089 (2016).

28. J. H. L. Voncken, "The Ore Minerals and Major Ore Deposits of the Rare Earths" in *The Rare Earth Elements: An Introduction*, J. H. L. Voncken, Ed. (Springer International Publishing, 2016), pp. 15–52.

29. H. Toyama, M. E. Lidstrom, pqqA is not required for biosynthesis of pyrroloquinoline quinone in Methylobacterium extorquens AM1. *Microbiology* **144 ( Pt 1)**, 183–191 (1998).

30. H. Lumpe, L. J. Daumann, Studies of Redox Cofactor Pyrroloquinoline Quinone and Its Interaction with Lanthanides(III) and Calcium(II). *Inorg. Chem.* **58**, 8432–8441 (2019).

31. N. M. Good, H. Lee, E. R. Hawker, A. A. Gilad, N. Cecilia Martinez-Gomez, Harnessing methylotrophs as a bacterial platform to reduce adverse effects of the use of the heavy lanthanide gadolinium in magnetic resonance imaging. *bioRxiv*, 2021.06.12.448192 (2021).

32. H. N. Vu, *et al.*, Lanthanide-Dependent Regulation of Methanol Oxidation Systems in Methylobacterium extorquens AM1 and Their Contribution to Methanol Growth. *J. Bacteriol.* **198**, 1250–1259 (2016).

33. N. M. Good, R. S. Moore, C. J. Suriano, N. C. Martinez-Gomez, Contrasting in vitro and in vivo methanol oxidation activities of lanthanide-dependent alcohol dehydrogenases XoxF1 and ExaF from Methylobacterium extorquens AM1. *Sci. Rep.* **9**, 4248 (2019).

34. W. Gu, J. D. Semrau, Copper and cerium-regulated gene expression in Methylosinus trichosporium OB3b. *Appl. Microbiol. Biotechnol.* **101**, 8499–8516 (2017).

35. S. Masuda, *et al.*, Lanthanide-Dependent Regulation of Methylotrophy in Methylobacterium aquaticum Strain 22A. *mSphere* **3**, e00462–17 (2018).

36. F. Chu, M. E. Lidstrom, XoxF Acts as the Predominant Methanol Dehydrogenase in the Type I Methanotroph Methylomicrobium buryatense. *J. Bacteriol.* **198**, 1317–1325 (2016).

37. C. L. M. Gilchrist, Y.-H. Chooi, Clinker & clustermap.js: Automatic generation of gene cluster comparison figures. *Bioinformatics* (2021) https:/doi.org/10.1093/bioinformatics/btab007.

38. C. L. M. Gilchrist, *et al.*, cblaster: a remote search tool for rapid identification and visualization of homologous gene clusters. *Bioinformatics Advances* **1** (2021).

39. D. B. Gladilovich, V. Kubán, L. Sommer, Determination of the sum of rare-earth elements by flow-injection analysis with Arsenazo III, 4-(2-pyridylazo)resorcinol, Chrome Azurol S and 5-bromo-2-(2-pyridylazo)-5-diethylaminophenol spectrophotometric reagents. *Talanta* **35**, 259–265 (1988).

40. D. B. Gladilovich, V. Kuban, Spectrophotometric determination of lanthanoids and yttrium by flow injection analysis using Chrome Azurol S in the presence of cationic surfactants. *Chem. Pap.* **42**, 607–620 (1988).

41. B. Schwyn, J. B. Neilands, Universal chemical assay for the detection and determination of siderophores. *Anal. Biochem.* **160**, 47–56 (1987).

42. Z. Shao, H. Zhao, H. Zhao, DNA assembler, an in vivo genetic method for rapid construction of biochemical pathways. *Nucleic Acids Res.* **37**, e16 (2009).

43. P. H. Brown, A. H. Rathjen, R. D. Graham, D. E. Tribe, "Chapter 92 Rare earth elements in biological systems" in *Handbook on the Physics and Chemistry of Rare Earths*, (Elsevier, 1990), pp. 423–452.

44. G. Tyler, Rare earth elements in soil and plant systems - A review. *Plant Soil* **267**, 191–206

(2004).

45. Z. Hu, H. Richter, G. Sparovek, E. Schnug, Physiological and Biochemical Effects of Rare Earth Elements on Plants and Their Agricultural Significance: A Review. *J. Plant Nutr.* **27**, 183–220 (2004).

46. R. Kastori R., I. Maksimovic V., T. Zeremski-Skoric M., M. Putnik-Delic I., Rare earth elements: Yttrium and higher plants. *Zb. Matice Srp. Prir. Nauk.*, 87–98 (2010).

47. I. Tamas, A. V. Smirnova, Z. He, P. F. Dunfield, The (d)evolution of methanotrophy in the Beijerinckiaceae--a comparative genomics analysis. *ISME J.* **8**, 369–382 (2014).

48. Y. Luo, *et al.*, Activation and characterization of a cryptic polycyclic tetramate macrolactam biosynthetic gene cluster. *Nat. Commun.* **4**, 2894 (2013).

49. S. Galanie, K. Thodey, I. J. Trenchard, M. Filsinger Interrante, C. D. Smolke, Complete biosynthesis of opioids in yeast. *Science* **349**, 1095–1100 (2015).

50. D. C. Bailey, E. J. Drake, T. D. Grant, A. M. Gulick, Structural and Functional Characterization of Aerobactin Synthetase IucA from a Hypervirulent Pathotype of Klebsiella pneumoniae. *Biochemistry* **55**, 3559–3570 (2016).

51. M. Miethke, A. J. Pierik, F. Peuckert, A. Seubert, M. A. Marahiel, Identification and characterization of a novel-type ferric siderophore reductase from a gram-positive extremophile. *J. Biol. Chem.* **286**, 2245–2260 (2011).

52. M. Miethke, M. A. Marahiel, Siderophore-based iron acquisition and pathogen control. *Microbiol. Mol. Biol. Rev.* **71**, 413–451 (2007).

53. X. Ge, *et al.*, Multiple pqqA genes respond differently to environment and one contributes dominantly to pyrroloquinoline quinone synthesis. *J. Basic Microbiol.* **55**, 312–323 (2015).

54. D. N. Nunn, M. E. Lidstrom, Isolation and complementation analysis of 10 methanol oxidation mutant classes and identification of the methanol dehydrogenase structural gene of Methylobacterium sp. strain AM1. *J. Bacteriol.* **166**, 581–590 (1986).

55. C. J. Marx, B. N. O'Brien, J. Breezee, M. E. Lidstrom, Novel methylotrophy genes of Methylobacterium extorquens AM1 identified by using transposon mutagenesis including a putative dihydromethanopterin reductase. *J. Bacteriol.* **185**, 669–673 (2003).

56. N. F. Delaney, *et al.*, Development of an optimized medium, strain and high-throughput culturing methods for Methylobacterium extorquens. *PLoS One* **8**, e62957 (2013).

57. G. Bertani, Studies on lysogenesis. I. The mode of phage liberation by lysogenic Escherichia coli. *J. Bacteriol.* **62**, 293–300 (1951).

58. N. M. Good, N. C. Martinez-Gomez, D. A. C. Beck, M. E. Lidstrom, Ethylmalonyl coenzyme A mutase operates as a metabolic control point in Methylobacterium extorquens

AM1. *J. Bacteriol.* **197**, 727–735 (2015).

59. A. P. Arkin, *et al.*, KBase: The United States Department of Energy Systems Biology Knowledgebase. *Nat. Biotechnol.* **36**, 566–569 (2018).

60. R. S. Sikorski, P. Hieter, A system of shuttle vectors and yeast host strains designed for efficient manipulation of DNA in Saccharomyces cerevisiae. *Genetics* **122**, 19–27 (1989).

61. H. Guo, S. A. Naser, G. Ghobrial, O. Phanstiel 4th, Synthesis and biological evaluation of new citrate-based siderophores as potential probes for the mechanism of iron uptake in mycobacteria. *J. Med. Chem.* **45**, 2056–2063 (2002).

62. Y.-H. Ho, S.-Y. Ho, C.-C. Hsu, J.-J. Shie, T.-S. A. Wang, Utilizing an iron(iii)-chelation masking strategy to prepare mono- and bis-functionalized aerobactin analogues for targeting pathogenic bacteria. *Chem. Commun.* **53**, 9265–9268 (2017).